Locating nonlinearities in mechanical systems

A frequency-domain dynamic network perspective

Classens, Koen; Schoukens, Maarten; Oomen, Tom; Noël, Jean Philippe

DOI
10.1016/j.ymssp.2024.112124

Publication date
2025

Document Version
Final published version

Published in
Mechanical Systems and Signal Processing

Citation (APA)
Classens, K., Schoukens, M., Oomen, T., & Noël, J. P. (2025). Locating nonlinearities in mechanical systems: A frequency-domain dynamic network perspective. *Mechanical Systems and Signal Processing*, *224*, Article 112124. https://doi.org/10.1016/j.ymssp.2024.112124

Mechanical Systems and Signal Processing 224 (2025) 112124

Contents lists available at ScienceDirect

Mechanical Systems and Signal Processing

journal homepage: www.elsevier.com/locate/ymssp

Full length article

Locating nonlinearities in mechanical systems: A frequency-domain dynamic network perspective

Koen Classens [a,*], Maarten Schoukens [b], Tom Oomen [a,c], Jean-Philippe Noël [d]

[a] Eindhoven University of Technology, Department of Mechanical Engineering, Control Systems Technology, Eindhoven, The Netherlands
[b] Eindhoven University of Technology, Department of Electrical Engineering, Control Systems, Eindhoven, The Netherlands
[c] Delft University of Technology, Department of Mechanical Engineering, Delft Center for Systems and Control, Delft, The Netherlands
[d] KU Leuven, Department of Mechanical Engineering, Robotics, Automation and Mechatronics (RAM), Leuven, Belgium

ARTICLE INFO

Communicated by D. Yurchenko

Keywords:
Nonlinear systems
Mechanical systems
System identification
Nonlinear data-driven modeling
Linearization
Dynamic networks

ABSTRACT

Accurately modeling nonlinearities is becoming increasingly important for mechanical systems, particularly in the context of system design, model-based control and monitoring systems for fault diagnosis. In the nonlinear modeling process, a pivotal phase involves pinpointing the physical locations and quantifying the magnitude of nonlinearities. This paper introduces a data-driven approach for nonlinearity location and quantification by analyzing nonparametric frequency response functions. To achieve this objective, measurement locations in mechanical systems are interpreted as nodes arranged in a dynamic network, and linearization techniques are employed on the frequency response functions formed from node to node. The efficacy of the proposed approach and the concept of nonlinearity localization and quantification are illustrated by numerical simulations and experiments on a flexible beam setup.

1. Introduction

The need for nonlinear models is increasingly acknowledged as a fundamental requirement in engineering disciplines. This acknowledgment is driven by the complex behavior of real-world systems, which often exceeds the capabilities of simplistic linear representations. A comprehensive understanding of nonlinear behavior is essential for various reasons. This understanding allows engineers to predict and mitigate potential problems during the design phase, such as structural instability or excessive vibrations [1]. On the other hand, nonlinearities can be strategically leveraged to overcome the performance limitations of linear systems, for instance, by novel mechanical design for vibration absorption [2], energy harvesting [3,4], or with nonlinear control [5,6]. However, many engineering systems, such as precision mechanics, are designed to exhibit dominant linear behavior. In these systems, the emergence of nonlinear behavior often serves as a symptomatic indicator of underlying faults. These faults can manifest in various forms, such as wear and tear, material degradation, or structural damage.

Detecting nonlinearities has wide-ranging applications across various domains, serving as a critical tool for monitoring, fault detection, damage assessment, and predictive maintenance [7,8]. To achieve these goals, it is essential not only to detect the presence of nonlinearities within the system, but also to quantify their magnitude and precisely pinpoint their location [9,10]. In the field of mechanics, complex nonlinearities such as friction [11], hysteresis [12], or contact nonlinearities [13] are frequently encountered and a nonlinearity location approach can be used as first step in the modeling or validation process for highly complex systems [14]. In addition to mechanics, locating nonlinearities is relevant for many other fields such as understand physiological processes in

* Corresponding author.
E-mail addresses: k.h.j.classens@tue.nl (K. Classens), m.schoukens@tue.nl (M. Schoukens), t.a.e.oomen@tue.nl (T. Oomen), jp.noel@kuleuven.be (J.-P. Noël).

https://doi.org/10.1016/j.ymssp.2024.112124
Received 3 June 2024; Received in revised form 30 October 2024; Accepted 3 November 2024
Available online 19 November 2024

biological systems [15], medical diagnosis and treatment, as well as enhancement of acoustical engineering. This interdisciplinary application underscores the significance of nonlinearity location across various fields and practical applications.

Many systems can be conceptualized as an interconnection of subsystems. Adopting the perspective of interconnected subsystems is known as the dynamic networks setting. Most of the research on identification in dynamic networks has focused on acquiring reliable estimates of linear subsystems, employing various techniques and considering different noise assumptions [16,17]. Further research on dynamic networks focuses on experiment design and input selection [18] or centers around topology detection techniques. For example, [19] describes the essential information required to recover the network structure from input–output data. Other approaches include Bayesian methods for sparse network reconstruction [20] or use distance functions specifically tailored for networks with tree topologies [21]. Beyond the identification of linear systems, substantial progress has been made in the identification of nonlinearities within mechanical systems in the last decade [22]. State-of-the-art methods enable the handling of strong nonlinearities in structural dynamics. For instance, both time-domain [23] and frequency-domain [24] subspace identification algorithms have been applied for nonlinear system identification. Only recently, frequency-domain identification and the dynamic network perspective were combined [25], allowing for detecting, locating, and quantifying nonlinearities in networks using linear approximation methods.

Although many advances have been made in the field of nonlinearity identification, many of these approaches require prior knowledge of the locations of the nonlinearities across the structure of interest. Another common aspect is the definition of an optimality criterion, which is only valid for a specified class of systems and under specific excitation signal conditions [26,27]. The existing literature on nonlinearity location is relatively limited [15,28] and, besides a nonlinear feedback perspective [29], lacks a solution for non-parametrically addressing this task. Given that many systems, including complex multi-input multi-output (MIMO) motion systems, primarily rely on non-parametric frequency response functions for modeling, there is a particular need for detecting, locating, and quantifying nonlinearities within this framework. Moreover, such approach offers considerable advantages, as experimental data is cheap to obtain and since it can be applied to a broad range of nonlinear systems with minimal reliance on prior assumptions and user input.

This article explores the detection, location, and quantification of nonlinearities using dynamic network theory and system identification, building upon the approach established in [25]. A detailed step-by-step procedure is outlined to guide the process, and the equivalences between mechanical systems and dynamic networks are illustrated. Additionally, the approach is validated experimentally. In this context, the Best Linear Approximation (BLA) [30,31], previously employed for nonlinearity detection [32,33], forms the foundation of the proposed method, however, is now utilized for pinpointing and quantifying nonlinearities. Specifically, the MIMO BLA framework [34,35] is integrated with the closed-loop [36,37] and process noise [38] framework. This establishes a comprehensive framework for networked systems.

The main contributions are summarized as follows:

- C1: A procedure is described to represent mechanical systems as dynamic networks, which is relevant for the identification of local modules and for locating and quantifying the magnitude of nonlinear elements.
- C2: A detailed step-by-step procedure is described to locate and quantify nonlinearities in MIMO mechanical systems. As outlined initially in [25], the procedure is based on frequency domain data and builds upon the BLA framework for MIMO systems.
- C3: The proposed method is evaluated through simulations and is experimentally validated on a flexible beam setup with a nonlinearity of varying magnitude.

The remainder of this article is organized as follows. In Section 2 dynamic networks are introduced, and the analogy between dynamic networks and mechanical systems is presented. Subsequently, the main problem is formulated. In Section 3 the concept of the BLA is revisited for open-loop single-input single-output (SISO) systems. Next, the focus is shifted to MIMO systems and a detailed step-by-step description of the proposed method for dynamic networks, based on the BLA concept, is given in Section 4. The proposed approach is numerically evaluated in Section 5, and applied to an experimental mechanical system in Section 6. Lastly, Section 7 concludes this paper.

2. System setup and problem formulation

In this section, the general framework of dynamic network identification tailored to mechanical systems is presented, leading to the formulation of the primary objective of this article.

2.1. Dynamic networks

Consider a dynamic network consisting of n_y nodes, as illustrated by the example in Fig. 1. These nodes represent the internal variables of the network. Within this network, the signal associated with each node, represented by $y_i(t)$, is computed as the sum of all incoming signals

$$y_i(t) = \sum_{j=1, j\neq i}^{n_y} y_{ij}(t) + y_{u_i}(t) + v_i(t), \tag{1}$$

where $y_{ij}(t)$ is the output of subsystem G_{ij}, and $y_{u_i}(t)$ is the output of the subsystem G_{u_i}, both pointing towards node i. The input of subsystem G_{ij} is the node signal $y_j(t)$ and the input of subsystem G_{u_i} is the external input $u_i(t)$. Each of the SISO subsystems may be linear or nonlinear. The remaining signal $v_i(t)$ denotes an additive process noise contribution that is assumed to be independent

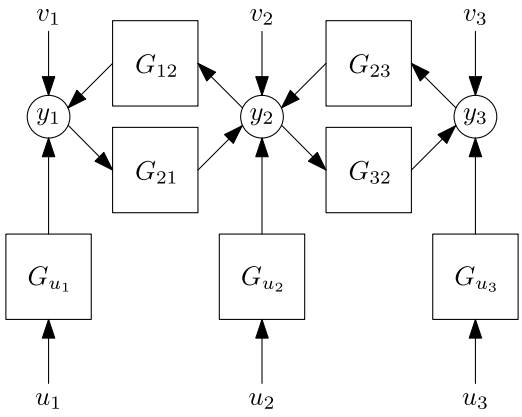

Fig. 1. A dynamic network consisting of three nodes, indicted with y_i, which are interconnected by dynamic subsystems G_{ij} and G_{u_i}. The node signals are calculated by summing all incoming signals. The exogenous incoming signals consist of the external inputs u_i and process noise contributions v_i.

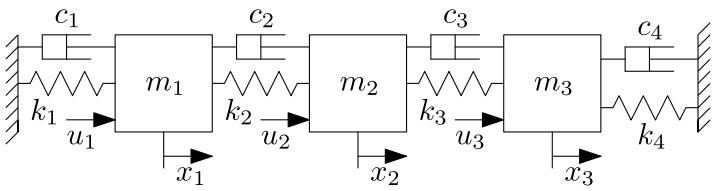

Fig. 2. A mechanical system with three masses m_i connected by four linear springs k_j and dampers c_j. The positions of the masses are indicated by x_i and a force u_i is applied to each mass.

of external inputs $u_j(t)$, $j \in 1, \dots, n_y$ and the other noise signals $v_k(t)$, $k \in 1, \dots, n_y$, where $k \neq i$. The noise signal $v_i(t)$ is assumed to be zero-mean and has a finite variance σ_{v_i}. This representation follows the definitions and visualization of [16,39]. Typically, only the node signals $y_i(t)$ and the input signals $u_i(t)$ are known.

Remark 2.1. Note that in this dynamic network framework, process noise is considered at the network nodes. Therefore, it differs from pure measurement noise, as the noise in this framework propagates through the submodels.

2.2. From mechanical system to dynamic network

An exact analogy can be made between mechanical systems with a discrete number of masses and a dynamic network. As an illustration, the underlying linear physical system of Fig. 2 is translated into a network representation.

The networked representation is based on the equations of motion,

$$m_1\ddot{x}_1(t) = -k_1x_1(t) - k_2(x_1(t) - x_2(t)) - c_1\dot{x}_1(t) - c_2(\dot{x}_1(t) - \dot{x}_2(t)) + u_1(t), \tag{2a}$$

$$m_2\ddot{x}_2(t) = -k_2(x_2(t) - x_1(t)) - k_3(x_2(t) - x_3(t)) - c_2(\dot{x}_2(t) - \dot{x}_1(t)) - c_3(\dot{x}_2(t) - \dot{x}_3(t)) + u_2(t), \tag{2b}$$

$$m_3\ddot{x}_3(t) = -k_3(x_3(t) - x_2(t)) - k_4x_3(t) - c_3(\dot{x}_3(t) - \dot{x}_2(t)) - c_4\dot{x}_3(t) + u_3(t), \tag{2c}$$

where $\ddot{x}(t) = \frac{\mathrm{d}^2x(t)}{\mathrm{d}t^2}$ and $\dot{x}(t) = \frac{\mathrm{d}x(t)}{\mathrm{d}t}$. Taking $p = \frac{\mathrm{d}}{\mathrm{d}t}$, and isolating $x_1(t)$, $x_2(t)$, and $x_3(t)$, allows to write the three equations of motion as

$$x_1(t) = \frac{k_2 + c_2p}{m_1p^2 + (c_1 + c_2)p + k_1 + k_2}x_2(t) + \frac{1}{m_1p^2 + (c_1 + c_2)p + k_1 + k_2}u_1(t), \tag{3a}$$

$$x_2(t) = \frac{k_2 + c_2p}{m_2p^2 + (c_2 + c_3)p + k_2 + k_3}x_1(t) + \frac{k_3 + c_3p}{m_2p^2 + (c_2 + c_3)p + k_2 + k_3}x_3(t) + \frac{1}{m_2p^2 + (c_2 + c_3)p + k_2 + k_3}u_2(t), \tag{3b}$$

$$x_3(t) = \frac{k_3 + c_3p}{m_3p^2 + (c_3 + c_4)p + k_3 + k_4}x_2(t) + \frac{1}{m_3p^2 + (c_3 + c_4)p + k_3 + k_4}u_3(t). \tag{3c}$$

This description of transfer functions admits the dynamic network representation in Fig. 1, where each position measurement $x_i(t)$ forms a node signal $y_i(t)$ which is perturbed by the node noise $v_i(t)$. The linear subsystems $G_{ij}(p)$ are formed by the relations between $x_i(t)$ and $x_j(t)$ and the linear subsystems $G_{u_i}(p)$ are formed by the relations between $x_i(t)$ and $u_i(t)$. Hence, after including the node noise, the node signals are formed by

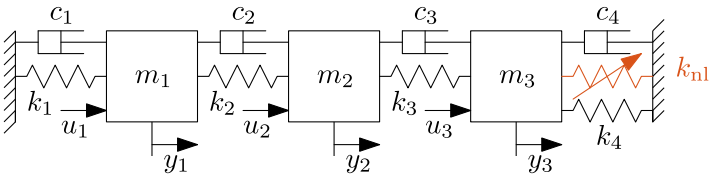

Fig. 3. A mechanical system with three masses connected by springs and dampers. In this example, a single nonlinear spring is present between the third mass and the fixed world. The positions of the masses are measured and a force is applied to each mass.

$$y_1(t) = G_{12}(p)y_2(t) + G_{u_1}(p)u_1(t) + v_1(t), \tag{4a}$$

$$y_2(t) = G_{21}(p)y_1(t) + G_{23}(p)y_3(t) + G_{u_2}(p)u_2(t) + v_2(t), \tag{4b}$$

$$y_3(t) = G_{32}(p)y_2(t) + G_{u_3}(p)u_3(t) + v_3(t), \tag{4c}$$

which indeed admits the visualization of Fig. 1.

In case nonlinear elements are present, see Fig. 3, the equations of motion will be nonlinear. As a result, the differential equations cannot be casted in the transfer function form which is a reasoning that applies only to linear systems. Still, the system can be represented as dynamic network where $y_{ij}(t)$ is the output of a (possibly) nonlinear subsystem G_{ij} with input y_j and $y_{u_i}(t)$ is the output of a (possibly) nonlinear subsystem G_{u_i} with input u_i. In this particular case, the node corresponding to y_3 will be connected to a nonlinear subsystems whereas the nodes y_1 and y_2 are only connected to linear elements. Hence, this particular system still admits the representation in Fig. 1.

Remark 2.2. The primary focus of this work is on mechanical systems, specifically mass–spring-damper systems. However, the proposed framework is applicable to a wide range of systems, including but not limited to electrical circuits, biological systems, hydraulic systems, and industrial process plants [40].

Remark 2.3. Consider the equations of motion of the system in Fig. 2. These are described by (3), which can be written in a matrix representation as

$$\begin{bmatrix} x_1(t) \\ x_2(t) \\ x_3(t) \end{bmatrix} = \underbrace{\begin{bmatrix} 0 & G_{12}(p) & G_{13}(p) \\ G_{21}(p) & 0 & G_{23}(p) \\ G_{31}(p) & G_{32}(p) & 0 \end{bmatrix}}_{:=G_x(p)} \begin{bmatrix} x_1(t) \\ x_2(t) \\ x_3(t) \end{bmatrix} + \underbrace{\begin{bmatrix} G_{u_1}(p) & 0 & 0 \\ 0 & G_{u_2}(p) & 0 \\ 0 & 0 & G_{u_3}(p) \end{bmatrix}}_{:=G_u(p)} \begin{bmatrix} u_1(t) \\ u_2(t) \\ u_3(t) \end{bmatrix},$$

where $G_{13}(p) = G_{31}(p) = 0$ since the first and third mass are not directly connected. The traditional MIMO system from inputs to outputs is represented as

$$\begin{bmatrix} x_1(t) \\ x_2(t) \\ x_3(t) \end{bmatrix} = \underbrace{\begin{bmatrix} S_{11}(p) & S_{12}(p) & S_{13}(p) \\ S_{21}(p) & S_{22}(p) & S_{23}(p) \\ S_{31}(p) & S_{32}(p) & S_{33}(p) \end{bmatrix}}_{:=S(p)} \begin{bmatrix} u_1(t) \\ u_2(t) \\ u_3(t) \end{bmatrix},$$

and relates to the networked representation via $S(p) = \left(I - G_x(p)\right)^{-1} G_u(p)$. The dynamics of the subsystems, i.e., the entries of $G_x(p)$ and $G_u(p)$, are all second order systems. The entries of $S(p)$ are all of sixth order. Hence, the dynamics of the entries in the networked representation are much simpler compared to the dynamics of the entries of $S(p)$, where the different second order entries are mixed together as a result of the inverse operator.

2.3. Problem formulation

Consider a dynamic network with n_y nodes, following the definitions in Section 2.1. The primary objective is to develop a data-driven method to determine the presence of nonlinearities and pinpoint their locations within a dynamic network. To this end, the node signals $y_i(t)$, $i \in 1, \dots, n_y$, are given, as well as the corresponding external inputs $u_i(t)$. The secondary objective is to quantify the extent or magnitude of these nonlinear effects.

The proposed method relies on the following assumptions:

Assumption 1. The system is a fading memory system and belongs to the PISPO (periodic in, same period out) system class [41] from the external excitation u_i to all the node signals y_i. For the PISPO system class, the steady-state response to a periodic excitation with period T is periodic with the same period T. Systems that produce sub-harmonics, operate with autonomous oscillations, undergo bifurcation, or exhibit chaos are not considered in this context. However, hard nonlinearities like clipping, dead zones, relays, and quantizers are permitted [38].

Fig. 4. The BLA represents a nonlinear system G using a LTI contribution G_{bla}, a stochastic nonlinear contribution y_s, and a noise source v.

Assumption 2. Every node i is excited by an independent external input u_i.

Remark 2.4. Despite these assumptions, nonlinearity location is possible for systems which do not satisfy Assumption 1 such as the duffing oscillator which behaves like a fading memory system within limited amplitude range or hysteretic systems, however, in that case the proposed approach for quantification does not directly apply.

3. Best linear approximation

Given the requirement for fast and reliable detection with limited user-intervention, a non-parametric approach is pursued. This section briefly reviews the robust BLA framework for open-loop SISO systems and how it is used for nonlinearity detection and quantification. In the next section, this framework is extended to networked systems.

3.1. System and signal class

As described in Section 2.3, the subsystems G_{ij}, G_{u_i}, have fading memory and belong to the PISPO system class [41]. Amongst others, this ensures that a periodic input applied to the system results, after a transient period, into a periodic output with the same periodicity as the input. A detailed mathematical treatment of these aspects is provided in [31].

The measured output signals of these (possibly nonlinear) systems, denoted by $y(t)$, are obtained as

$$y(t) = y_0(t) + v(t), \tag{5}$$

where $y_0(t)$ is the noiseless system output of the nonlinear dynamic system with input $u(t)$, and $v(t)$ is a, possibly colored, zero-mean, finite-variance noise signal, see Fig. 4.

The zero-mean random phase multisine input signal class is considered in the next sections. Random phase multisines give the user full control over the amplitude spectrum, but have random phases. Their periodic nature is key in term of noise and nonlinearity characterization. Random phase multisines belong to the Riemann-equivalence class of excitation signals. This class contains all signals that are (asymptotically) Gaussian distributed, and have the same power on each finite frequency interval (for the number of samples and excited frequencies growing to infinity) [42]. A random multisine signal is defined as

$$u(t) = \frac{1}{\sqrt{N}} \sum_{k=1}^{N/2-1} U_k \cos\left(2\pi k f_0 t + \phi_k\right), \tag{6}$$

where the phase ϕ_k is uniformly independently random distributed such that $\mathbb{E}\{e^{j\phi_k}\} = 0$, N is the total number of points per period, and f_0 is the frequency resolution. For f_s being the sampling frequency and T being the period length, $f_0 = f_s/N = 1/T$. A common choice is to select the phases such that they are uniformly distributed between $[0, 2\pi)$. The amplitudes U_k can be chosen to follow a desired amplitude spectrum.

3.2. Best linear approximation definition

The BLA framework approximates a nonlinear system with zero-mean (colored) additive output noise, i.e., following (5), using a linear time-invariant (LTI) model. The BLA is defined in [30,31] as the LTI model that minimizes the expected least-squares difference between the measured and the modeled output, hence

$$G_{\text{bla}}(q) = \underset{G(q)}{\arg\min}\, \mathbb{E}_{u,v}\left\{\left|\tilde{y}(t) - G(q)\,\tilde{u}(t)\right|^2\right\}, \tag{7}$$

where

$$\tilde{u}(t) = u(t) - \mathbb{E}_u\{u(t)\}, \tag{8}$$

$$\tilde{y}(t) = y(t) - \mathbb{E}_{u,v}\{y(t)\}. \tag{9}$$

Here $\mathbb{E}_{u,v}\{\cdot\}$ denotes the expected value operator with respect to the random variations due to the input $u(t)$ and the output noise $v(t)$, and $G(q)$ belongs to the set of all possible LTI systems.

The approximation of a nonlinear system with $G_{\text{bla}}(q)$ is visualized in Fig. 4. The approximation is the sum of three elements, namely the output of G_{bla}, and 2 distinct disturbance contributions. These disturbances are the noise distortion $v(t)$, which is commonly present in the LTI literature, and the stochastic nonlinear distortion $y_s(t)$, also referred to as the noncoherent output [42], hence,

$$y(t) = G_{\text{bla}}(q)u(t) + y_s(t) + v(t). \tag{10}$$

Equivalently, using a frequency-domain notation the BLA is obtained from

$$G_{\text{bla}}(\omega_k) = \underset{G(\omega_k)}{\arg\min}\, \mathbb{E}_{u,v}\left\{ \left| \tilde{y}(\omega_k) - G(\omega_k)\, \tilde{u}(\omega_k) \right|^2 \right\}, \tag{11}$$

where the approximation consists of the same three contributions, i.e.,

$$y(\omega_k) = G_{\text{bla}}(\omega_k)u(\omega_k) + y_s(\omega_k) + v(\omega_k), \tag{12}$$

with $\omega_k = 2\pi k f_0$.

The total distortion consisting of the stochastic nonlinear distortion, representing the unmodeled nonlinear contributions, and the noise contribution is consequently obtained by subtracting the contribution of the best linear estimate from the output as

$$y_t(\omega_k) = y(\omega_k) - G_{\text{bla}}(\omega_k)u(\omega_k) = y_s(\omega_k) + v(\omega_k). \tag{13}$$

The contributions of $y_s(\omega_k)$ and $v(\omega_k)$ can be separated since the nonlinear distortion $y_s(t)$ is linearly uncorrelated with the input $\tilde{u}(t)$, i.e., $\left(\mathbb{E}_u\{y_s(t)\tilde{u}(\tau)\} = 0\ \forall t, \tau\right)$, however, it is not independent of $\tilde{u}(t)$. On the contrary, the noise distortion $v(t)$ is both uncorrelated, i.e., $\left(\mathbb{E}_u\{v(t)\tilde{u}(\tau)\} = 0\ \forall t, \tau\right)$, and independent of the input $\tilde{u}(t)$. This fundamental difference enables the separation of nonlinear effects. Hence, the nonlinear distortion and the noise distortion equal

$$y_s(\omega_k) = y_0(\omega_k) - G_{\text{bla}}(\omega_k)u(\omega_k), \tag{14}$$

$$v(\omega_k) = y(\omega_k) - G_{\text{bla}}(\omega_k)u(\omega_k) - y_s(\omega_k). \tag{15}$$

The nonlinearity of a system can be quantified by the variance of the nonlinear distortion. For this variance estimate the robust BLA approach can be used [31].

3.3. Measuring the BLA: the robust approach

Two main approaches are available in the literature to determine the BLA and obtain an estimate of the variances of the stochastic and noise distortion contributions: the so-called fast approach and robust approach [31]. This section briefly recapitulates the main aspects of the robust approach, as it forms the basis of the proposed nonlinearity location and quantification algorithm.

The key observation that enables the separation between noise and the nonlinear disturbances is that the noise behaves aperiodic, while the nonlinear disturbances behave periodic for PISPO systems that are excited by a periodic input. The robust approach relies on applying M different realizations of a random phase multisine signal, see (6), with the same power spectrum and measure P steady-state periods of each experiment. For each period of each realization, the frequency response function (FRF) is calculated as

$$\hat{G}_{\text{bla}}^{[m,p]}(\omega_k) = \frac{\tilde{y}^{[m,p]}(\omega_k)}{\tilde{u}^{[m,p]}(\omega_k)}, \tag{16}$$

where $\tilde{y}^{[m,p]}(\omega_k)$ and $\tilde{u}^{[m,p]}(\omega_k)$ denote the leakage-free discrete fourier transform (DFT) of the pth period and the mth realization of the input and output signals $\tilde{y}(t)$ and $\tilde{u}(t)$ respectively. The sample mean over the P periods is then computed as

$$\hat{G}_{\text{bla}}^{[m]}(\omega_k) = \frac{1}{P}\sum_{p=1}^{P} \hat{G}_{\text{bla}}^{[m,p]}(\omega_k). \tag{17}$$

Subsequently, taking the sample mean over the M realizations gives the BLA estimate as

$$\hat{G}_{\text{bla}}(\omega_k) = \frac{1}{M}\sum_{m=1}^{M} \hat{G}_{\text{bla}}^{[m]}(\omega_k). \tag{18}$$

The sample variance can be taken over the P periods to obtain the variance as a result of noise for the mth experiment as

$$\sigma^{2}_{G^{[m]}_{\text{bla},v}}(\omega_k) = \frac{1}{P(P-1)}\sum_{p=1}^{P} \left| \hat{G}_{\text{bla}}^{[m,p]}(\omega_k) - \hat{G}_{\text{bla}}^{[m]}(\omega_k) \right|^2. \tag{19}$$

The sample variance can also be computed of the M realizations in order to examine the combined effect due to noise and nonlinearities on the averaged BLA as

$$\sigma^2_{G_{\text{bla},t}}(\omega_k) = \frac{1}{M(M-1)}\sum_{m=1}^{M} \left| \hat{G}_{\text{bla}}^{[m]}(\omega_k) - \hat{G}_{\text{bla}}(\omega_k) \right|^2, \tag{20}$$

where the subscript of $\sigma^2_{G_{\text{bla},t}}(\omega_k)$ refers to the total effect. Hence, taking the variance over the periods quantifies the noise level in the measurements. Taking the variance over the different realizations quantifies the combined influence of the nonlinearities and

the noise on the FRF. The variance in (19) only considers one experiment. Taking the mean of this sample variance over the M experiments gives the noise variance on the averaged BLA as

$$\sigma^2_{G_{\text{bla},v}}(\omega_k) = \frac{1}{M^2}\frac{1}{P(P-1)}\sum_{m=1}^{M}\sum_{p=1}^{P}\left|\hat{G}^{[m,p]}_{\text{bla}}(\omega_k) - \hat{G}^{[m]}_{\text{bla}}(\omega_k)\right|^2. \tag{21}$$

The estimate of the variance due to the stochastic nonlinear distortion y_s, can now be separated, and is given by

$$\sigma^2_{G_{\text{bla},s}}(\omega_k) = \begin{cases} \left(\sigma^2_{G_{\text{bla},t}}(\omega_k) - \sigma^2_{G_{\text{bla},v}}(\omega_k)\right) & \text{if } \sigma^2_{G_{\text{bla},t}}(\omega_k) > \sigma^2_{G_{\text{bla},v}}(\omega_k), \\ 0 & \text{if } \sigma^2_{G_{\text{bla},t}}(\omega_k) \le \sigma^2_{G_{\text{bla},v}}(\omega_k). \end{cases} \tag{22}$$

Remark 3.1. Note that the variances are so-called sample variances explaining the $P-1$ and $M-1$ factors. In order to quantify the variability of the *mean* BLA estimate (18), extra factors M and P have been introduced in the sample variances (19) and (20). These BLA estimate variances can be scaled back to the output level to obtain the estimates of the variance of y_s and v using

$$\sigma^2_{y_s}(\omega_k) = M\sigma^2_{\text{bla},s}\left|u(\omega_k)\right|^2, \tag{23}$$

$$\sigma^2_{v}(\omega_k) = MP\sigma^2_{\text{bla},v}\left|u(\omega_k)\right|^2. \tag{24}$$

The system under test is considered to be nonlinear in case a nonzero $\sigma^2_{y_s}(\omega_k)$ variance is present. Since this is a variance estimate over the different frequencies, one can also observe in which frequency range the system is most nonlinear.

4. Nonlinearity location methodology

The BLA approach presented in Section 3 is posed for open-loop SISO systems and enables the detection and quantification of nonlinearities. In contrast, for pinpointing the origin of nonlinearities in MIMO systems, the system has to be considered in the framework of dynamic networks. A key assumption to properly apply the standard BLA framework is that the noise sources disturbing the input and the output of each subsystem must be uncorrelated. This assumption is violated in a dynamic network because the noise sources propagate through the subsystems. Consequently, the BLA of the network cannot be calculated directly.

To circumvent this issue, a three-step methodology is followed, first introduced in [25]. Instead of estimating the BLA of an open-loop SISO system, the method aims to identify the BLA of the subsystems present in the nonlinear dynamic network. To identify the network nodes that are directly connected to nonlinear elements, the measured node-to-node dynamics are linearized using the BLA framework as conceptually visualized in Fig. 5. This is achieved by combining the BLA framework for systems operating in closed loop [37] and the BLA framework for process noise [38], and the BLA framework for MIMO systems [34,35]. The noise variance and the stochastic nonlinear distortion variance are computed of every network node signal. This multi-stage approach avoids the introduction of bias as a result of correlated noise contributions due to the presence of feedback loops in the dynamic network.

In summary, the proposed methodology for nonlinearity location comprises three primary steps, which will be elaborated upon in the following subsections.

1. Calculate the BLA from inputs to nodes and simulate the noise-free linearized system outputs;
2. Calculate the BLA from nodes to nodes and simulate the node-to-node approximate dynamics;
3. Conduct a residual analysis along the frequency axis using the variance of the total distortions $\sigma^2_{t,i}(\omega_k)$ and the variance of the noise distortions $\sigma^2_{v,i}(\omega_k)$. Any difference is attributed to a nonlinearity-induced variance. In contrast to the standard BLA approach, the residual analysis is performed at the signal level instead of on the basis of FRFs.

4.1. Step 0: Measurements and data generation

To perform the networked BLA analysis, the dynamics between the network nodes have to be estimated. To this end, all the network nodes are excited simultaneously using orthogonal multisine excitations, as outlined in [43]. Note that the network nodes also function as the system outputs, and thus an equal amount of inputs and outputs is used, i.e., $n_u = n_y$.

Similar to the random phase multisine introduced in Section 3, the user first selects the frequencies to be excited and a random phase multisine signal is generated for each input u_i. To perform MIMO FRF identification with n_u inputs and outputs, n_u experiments are constructed of which the inputs are stacked as

$$U(\omega_k) = \begin{bmatrix} u_{1,1}(\omega_k) & u_{1,2}(\omega_k) & \dots & u_{1,n_u}(\omega_k) \\ u_{2,1}(\omega_k) & u_{2,2}(\omega_k) & \dots & u_{2,n_u}(\omega_k) \\ \vdots & \vdots & \ddots & \vdots \\ u_{n_u,1}(\omega_k) & u_{n_u,2}(\omega_k) & \dots & u_{n_u,n_u}(\omega_k) \end{bmatrix}, \tag{25}$$

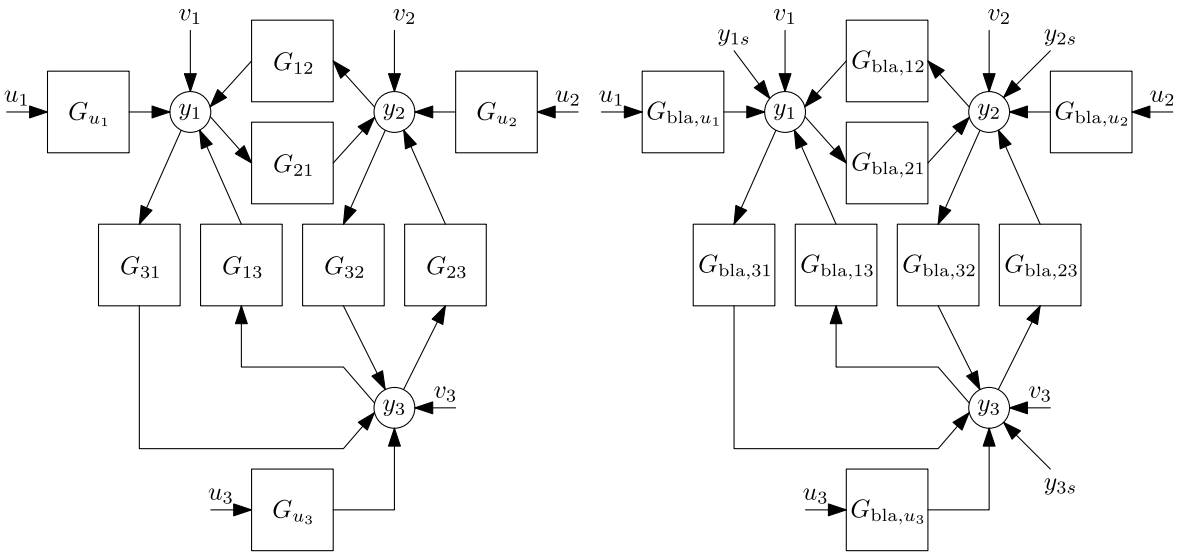

Fig. 5. A fully populated nonlinear dynamic network (left) and its BLA (right). The BLA represent the nonlinear network modules G_{ij} using LTI models denoted as $G_{\text{bla},ij}$. Furthermore, y_{is} corresponds to a stochastic nonlinear contribution, and v_i corresponds to a noise source.

with $u_{i,c} = e^{-\frac{j2\pi(i-1)(c-1)}{n_y}} u_i$ describing the orthogonal multisine excitation, where i refers to the input channel number and c refers to the experiment number. Hence, each row denotes a particular input channel and each column represents a new experiment. The resulting output data is stacked similarly as

$$Y(\omega_k) = \begin{bmatrix} y_{1,1}(\omega_k) & y_{1,2}(\omega_k) & \dots & y_{1,n_y}(\omega_k) \\ y_{2,1}(\omega_k) & y_{2,2}(\omega_k) & \dots & y_{2,n_y}(\omega_k) \\ \vdots & \vdots & \ddots & \vdots \\ y_{n_y,1}(\omega_k) & y_{n_y,2}(\omega_k) & \dots & y_{n_y,n_y}(\omega_k) \end{bmatrix}, \tag{26}$$

where $y_{i,c}$ refers to the ith output channel and the cth experiment.

Remark 4.1. Note that two distinct notations are used in the subscripts. Comma-separated supscripts such as $y_{i,c}$ indicate the ith output channel and the cth experiment, whereas y_{ij} indicates the internal signal from node j to node i.

In total M realizations and $\tilde{P}$ periods of this combined experiment will executed. Of the $\tilde{P}$ periods, the last $P = \tilde{P} - \tilde{P}_{\text{transient}}$ steady state periods are used, i.e., the first $\tilde{P}_{\text{transient}}$ periods are discarded. Here, $Y^{[m,p]}(\omega_k)$ and $U^{[m]}(\omega_k)$ denote the mth realization and pth period of the combined experiment, and similarly $y_{i,c}^{[m,p]}(\omega_k)$ and $u_{i,c}^{[m]}(\omega_k)$ denote its entries. The p index is dropped for the input signals, as they are identical over all periods. Hence, a total of Mn_y experiments are performed, each containing PN steady-state samples.

4.2. Step 1: BLA analysis from inputs to nodes

The first step consists of calculating the MIMO BLA from all external inputs to the node signals. The BLA of a subsystem, represented by $S_{\text{bla},ij}(\omega_k)$, captures the relationship from input j to node i with a transfer function, offering the best linear approximation in a least-squares sense. The complete $n_y \times n_u$ BLA, labeled as $S_{\text{bla}}(\omega_k)$, is determined from

$$S_{\text{bla}}(\omega_k) = \underset{S(\omega_k)}{\arg\min}\, \mathbb{E}_{u,v} \left\{ \sum_{i=1}^{n_y} \left| \tilde{y}_i(\omega_k) - \sum_{j=1}^{n_u} S_{ij}(\omega_k)\, \tilde{u}_j(\omega_k) \right|^2 \right\}. \tag{27}$$

The expectation $\mathbb{E}_{u,v}\{\cdot\}$ is taken with respect all possible realizations of the input signals u_j and noise signals v_i, within the considered signal class.

In practice this is realized by computing

$$\hat{S}_{\text{bla}}(\omega_k) = \frac{1}{MP} \sum_{m=1}^{M} \sum_{p=1}^{P} \tilde{Y}^{[m,p]}(\omega_k) \tilde{U}^{[m,p]^{-1}}(\omega_k), \tag{28}$$

where $\tilde{Y}$ and $\tilde{U}$ are the zero-mean equivalent signals of (25) and (26), and thus

$$\hat{S}_{\text{bla}}(\omega_k) = \begin{bmatrix} S_{\text{bla},11}(\omega_k) & S_{\text{bla},12}(\omega_k) & \dots & S_{\text{bla},1n_u}(\omega_k) \\ S_{\text{bla},21}(\omega_k) & S_{\text{bla},22}(\omega_k) & \dots & S_{\text{bla},2n_u}(\omega_k) \\ \vdots & \vdots & \ddots & \vdots \\ S_{\text{bla},n_y1}(\omega_k) & S_{\text{bla},n_y2}(\omega_k) & \dots & S_{\text{bla},n_yn_u}(\omega_k) \end{bmatrix}. \tag{29}$$

The obtained BLA estimate (27) allows to calculate a noise-free and nonlinear distortion-free linear approximation $\bar{y}_i(\omega_k)$ of the node signal $y_i(\omega_k)$. In particular, $\bar{y}_{i,c}(\omega_k)$ and $y_{i,c}(\omega_k)$ denote the frequency content of the signals corresponding to the cth experiment. The approximated incoming signals of node i are computed through

$$\bar{y}_{i,c}^{[m]}(\omega_k) = \sum_{j=1}^{n_y} \hat{S}_{\text{bla},ij}(\omega_k) u_{j,c}^{[m]}(\omega_k). \tag{30}$$

4.3. Step 2: BLA analysis from nodes to nodes

A second FRF estimation is carried out to obtain the estimates between nodes, considering the noise-free node signals $\bar{y}_i$ as inputs, and taking into account the direct contributions of the forcing signals u_i. This results in BLA estimates $G_{\text{bla},ij}(\omega_k)$ from node j to node i and $G_{\text{bla},iu}(\omega_k)$ from the system input i to node i, obtained from

$$G_{\text{bla},ij}(\omega_k),\ G_{\text{bla},u_i}(\omega_k) = \underset{G_{ij},\, G_{u_i}}{\arg\min}\, \mathbb{E}_{u,v} \left\{ \left| \sum_{i=1}^{n_y} \left| \bar{y}_i(\omega_k) - G_{u_i}(\omega_k) u_i(\omega_k) - \sum_{j=1,\, j\neq i}^{n_y} G_{ij}(\omega_k)\, \bar{y}_j(\omega_k) \right|^2 \right\}. \tag{31}$$

In practice, the estimates per node are obtained as

$$\hat{G}_{\text{bla},i}(\omega_k) = \frac{1}{M} \sum_{m=1}^{M} \bar{Y}_i^{[m]}(\omega_k) {Z_i^{[m]}}^{-1}(\omega_k), \tag{32}$$

where

$$\hat{G}_{\text{bla},i}(\omega_k) = \begin{bmatrix} G_{\text{bla},u_i}(\omega_k) & G_{\text{bla},i1}(\omega_k) & \dots & G_{\text{bla},i(i-1)}(\omega_k) & G_{\text{bla},i(i+1)}(\omega_k) & \dots & G_{\text{bla},in_y}(\omega_k) \end{bmatrix}, \tag{33}$$

$$\bar{Y}_i^{[m]}(\omega_k) = \begin{bmatrix} \bar{y}_{i,1}(\omega_k) & \bar{y}_{i,2}(\omega_k) & \dots & \bar{y}_{i,n_y}(\omega_k) \end{bmatrix}, \tag{34}$$

$$Z_i^{[m]}(\omega_k) = \begin{bmatrix} u_{i,1}(\omega_k) & u_{i,2}(\omega_k) & \dots & u_{i,n_y}(\omega_k) \\ \bar{y}_{1,1}(\omega_k) & \bar{y}_{1,2}(\omega_k) & \dots & \bar{y}_{1,n_y}(\omega_k) \\ \vdots & \vdots & \ddots & \vdots \\ \bar{y}_{i-1,1}(\omega_k) & \bar{y}_{i-1,2}(\omega_k) & \dots & \bar{y}_{i-1,n_y}(\omega_k) \\ \bar{y}_{i+1,1}(\omega_k) & \bar{y}_{i+1,2}(\omega_k) & \dots & \bar{y}_{i+1,n_y}(\omega_k) \\ \vdots & \vdots & \ddots & \vdots \\ \bar{y}_{n_y,1}(\omega_k) & \bar{y}_{n_y,2}(\omega_k) & \dots & \bar{y}_{n_y,n_y}(\omega_k) \end{bmatrix}. \tag{35}$$

Note that (32) to (35) are calculated for each node separately.

The frequency content of the node signals can now be calculated using the node-to-node and input-to-node linear approximate description $G_{\text{bla},ij}(\omega_k)$, $G_{\text{bla},u_i}(\omega_k)$ of the network dynamics as

$$\bar{\bar{y}}_{i,c}^{[m,p]}(\omega_k) = G_{\text{bla},u_i}(\omega_k) u_{i,c}(\omega_k) + \sum_{j=1, j\neq i}^{n_y} G_{\text{bla},ij}(\omega_k) y_{j,c}^{[m,p]}(\omega_k). \tag{36}$$

Observe that the difference between $\bar{\bar{y}}_{i,c}^{[m,p]}$ and $y_{i,c}^{[m,p]}$ is the noise and stochastic nonlinear contribution on that particular node, the noise and stochastic nonlinearity contributions on node i coming from the other nodes have been taken into account as they are present in the measured $y_{j,c}^{[m,p]}$ signal. This allows for the nonlinearity location through residual analysis in the next subsection.

4.4. Step 3: Residual analysis and nonlinearity location

By comparing the simulated node signals $\bar{\bar{y}}_{i,c}^{[m,p]}$ and the corresponding measurements $y_{i,c}^{[m,p]}$ over multiple periods and realizations, a residual analysis can be conducted. In contrast to the classical BLA analysis discussed in Section 3, where variances are computed based of the mean BLA, in this context, variances are computed of the residuals signals. For the analysis, the phase-rotated experiments, indicated with subscript c, are stacked for each realization m. To this end, consider $\bar{\bar{y}}_i^{[\tilde{m},p]}$ and $y_i^{[\tilde{m},p]}$, with $\tilde{m} = 1, \dots, \tilde{M}$ and $\tilde{M} = Mn_y$.

Considering the residual $e_i^{[\tilde{m},p]}(\omega_k) = \bar{\bar{y}}_i^{[\tilde{m},p]}(\omega_k) - y_i^{[\tilde{m},p]}(\omega_k)$ at node i, the variances of the total distortions $\sigma_{t,i}^2(\omega_k)$, the variance of the noise distortions $\sigma_{v,i}^2(\omega_k)$, and the variance of the nonlinear distortions $\sigma_{s,i}^2(\omega_k)$ are separated following a similar reasoning as in Section 3.3. Hence, averaging over the periods P and realizations $\tilde{M}$ gives

$$e_i^{[\tilde{m}]}(\omega_k) = \frac{1}{P}\sum_{p=1}^{P} e_i^{[\tilde{m},p]}(\omega_k), \tag{37}$$

$$e_i^{[p]}(\omega_k) = \frac{1}{\tilde{M}}\sum_{\tilde{m}=1}^{\tilde{M}} e_i^{[\tilde{m},p]}(\omega_k). \tag{38}$$

The total distortion due to noise and stochastic nonlinearities, $\sigma^2_{t,i}(\omega_k)$, is obtained by taking the variance of the residuals over the realizations. The noise distortion, $\sigma^2_{n,i}(\omega_k)$, is obtained by taking the variance of the residuals over the periods. The stochastic contribution, $\sigma^2_{s,i}(\omega_k)$, can then be obtained by taking the difference of these two.

In frequency domain, the total distortion equals

$$\sigma^2_{t,i}(\omega_k) = \frac{1}{P(\tilde{M}-1)}\sum_{p=1}^{P}\sum_{\tilde{m}=1}^{\tilde{M}}\left(e_i^{[\tilde{m},p]}(\omega_k) - e_i^{[p]}(\omega_k)\right)^2, \tag{39}$$

and the variance due to noise equals

$$\sigma^2_{v,i}(\omega_k) = \frac{1}{\tilde{M}(P-1)}\sum_{\tilde{m}=1}^{\tilde{M}}\sum_{p=1}^{P}\left(e_i^{[\tilde{m},p]}(\omega_k) - e_i^{[\tilde{m}]}(\omega_k)\right)^2. \tag{40}$$

With these, the variance due to stochastic nonlinearities is obtained from the difference, i.e.,

$$\sigma^2_{s,i}(\omega_k) = \begin{cases} \sigma^2_{t,i}(\omega_k) - \sigma^2_{v,i}(\omega_k) & \text{if } \sigma^2_{t,i}(\omega_k) > \sigma^2_{v,i}(\omega_k), \\ 0 & \text{if } \sigma^2_{t,i}(\omega_k) \leq \sigma^2_{v,i}(\omega_k). \end{cases} \tag{41}$$

The level of the estimated nonlinear variance $\sigma^2_{s,i}$ quantifies the nonlinear distortion at each network node. With the nonlinearity levels at each node, the nonlinear part of the dynamic network can be pinpointed by comparison between the nodes. If no nonlinearity is present at a given node, the total distortion equals the noise distortion.

5. Simulation study

This section demonstrates the proposed three-step nonlinearity location method from Section 4 applied to the three-mass system from Fig. 3 where the nonlinear element between the third mass and the fixed world is a cubic spring. Before applying the three-step method, the classical MIMO BLA framework is applied to illustrate that the classical method does not allow nonlinearity location, but only detection.

The physical properties of the system are equal to $m_1 = 1$ kg, $m_2 = 0.8$ kg, and $m_3 = 1.2$ kg, with spring constants $k_1 = 2 \cdot 10^4$ N/m, $k_2 = 3.5 \cdot 10^4$ N/m, $k_3 = 5 \cdot 10^4$ N/m, and $k_4 = 8 \cdot 10^4$ N/m. The nonlinear spring constant $k_{\text{nl}} = 1 \cdot 10^8$ N/m^3, and the damping constants are uniformly assigned as $c_1 = c_2 = c_3 = c_4 = 8$ Ns/m.

The system is excited with three multisines which are simultaneously applied to the three masses, which are initialized at zero. These signals excite the system at all frequencies in the 5–100 Hz frequency range with a root-mean-square amplitude of 50 N and a random uniformly distributed phase. The position signals, i.e., the node signals, are generated using a nonlinear Newmark integration algorithm [44] with a sampling frequency of 5000 Hz. Each experiment has 4 periods with $N = 8192$ samples each. The experiment is repeated for $M = 10$ different realizations, i.e., $\tilde{M} = 30$ experiments, of which the last $P = 2$ steady-state periods are used for the following analysis. The resulting displacement is measured and corrupted with a white Gaussian noise signal such that the signal-to-noise ratio is 40 dB.

First, the BLA estimate $\hat{S}_{\text{bla}}$ is computed from the inputs to the nodes using the robust BLA method, i.e., (28) in practice. This BLA is depicted in Fig. 6 together with the underlying system without nonlinearity.

Nonlinearities can be detected and quantified in the classical MIMO BLA setting from inputs to network nodes. This can be achieved using the analysis presented in Section 4.4, but with residuals based on $\bar{y}_{i,c}^{[m,p]}$ obtained from (30) instead of $\bar{y}_{i,c}^{[m,p]}$. The resulting node signals and distortions are presented in Fig. 7. The nonlinear distortion is above the noise distortion for all network nodes indicating dominant nonlinear behavior. Yet, only a single nonlinear element is present. Therefore, the traditional input-to-node BLA analysis is not adequate for pinpointing the location of the nonlinear element.

Next, the node-to-node BLA $\hat{G}_{\text{bla}}$ is estimated using (32). This BLA is depicted in Fig. 8 together with the underlying true node-to-node dynamics corresponding to the imposed dynamic network structure from Fig. 1. Note that these node-to-node dynamics are of low order compared to the dynamics from the inputs to the nodes in Fig. 6, c.f. (3), and that the imposed dynamic network does not include the entries $\hat{G}_{\text{bla},13}$ and $\hat{G}_{\text{bla},31}$.

Finally, the approach for the detection, location and quantification of Section 4.4 is applied. The result is depicted in Fig. 9, which reveals that the nonlinear distortion is smaller compared to the noise distortion at nodes 1 and 2, suggesting predominantly linear system behavior of the connected elements. In sharp contrast, at node 3, the situation is reversed, indicating dominant nonlinear distortions compared to the noise distortion. In conclusion, from Fig. 9 is inferred that a nonlinear element affects the three-mass system dynamics, and that it is attached to the third mass 3 on one side and grounded on the other side. Note that due to the nature of the elements present in the example, i.e., springs and dampers, it is evident that no nonlinear element is present between the second and third mass as such nonlinear element would result in a nonlinear distortion affecting the second node.

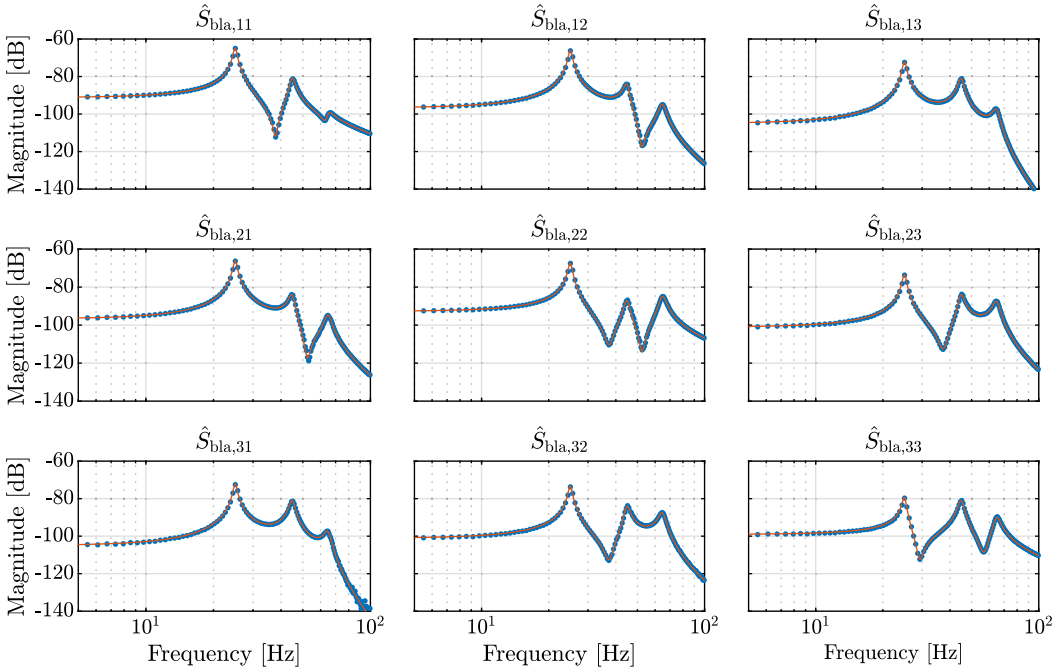

Fig. 6. The BLA from the inputs to nodes $\hat{S}_{\text{bla}}$ (•) of the three mass–spring-damper system with cubic spring from Fig. 3 and the true underlying system without nonlinearity, i.e., S with $k_{\text{nl}} = 0$ (—).

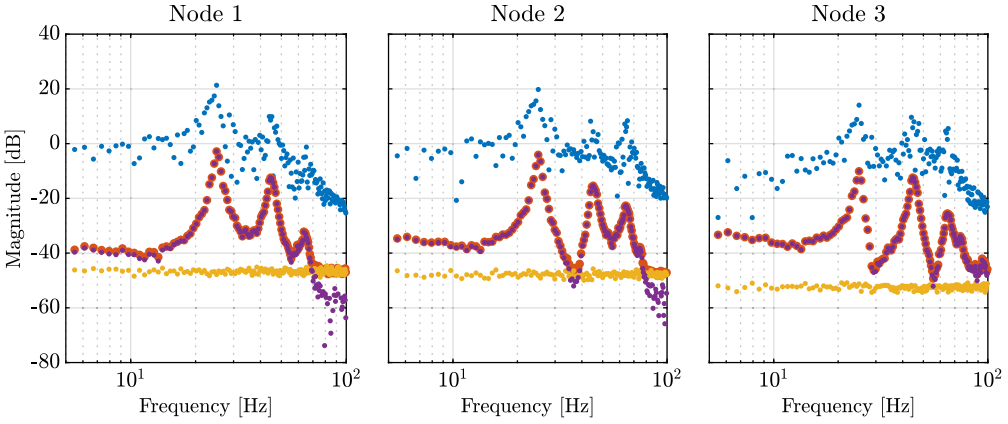

Fig. 7. Nonlinearity detection in the three-mass–spring-damper system using the classical input-to-node dynamics. The spectra of the node signals $y_i(\omega_k)$ (•), the total distortion levels $\sigma^2_{t,i}(\omega_k)$ (•), the distortions due to noise $\sigma^2_{v,i}(\omega_k)$ (•), and the nonlinear distortions $\sigma^2_{s,i}(\omega_k)$ (•), are depicted. Since the nonlinear distortion is above the noise floor, dominant nonlinearity is detected.

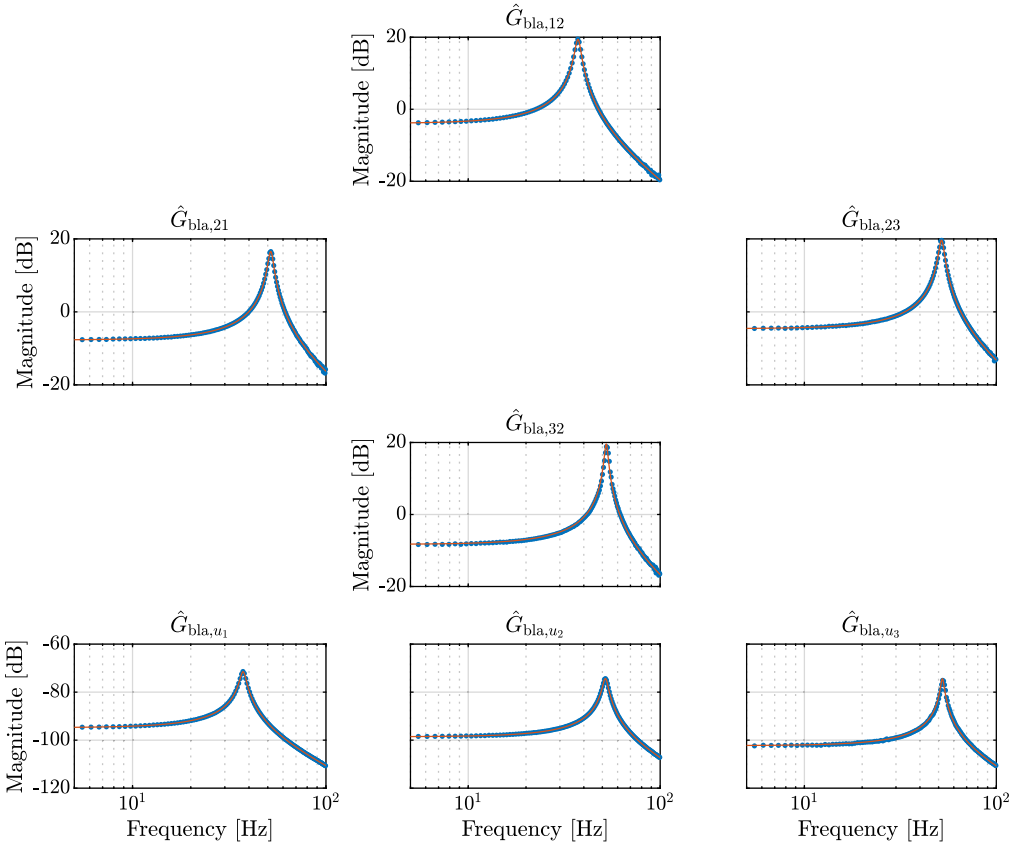

Fig. 8. The BLA of the node-to-node dynamics $\hat{G}_{\text{bla}}$ (•) of the three mass–spring-damper system from Fig. 3 and the true underlying node-to-node dynamics with $k_{\text{nl}} = 0$ (——). Note that the imposed dynamic network structure from Fig. 1 does not include the entries $\hat{G}_{\text{bla},13}$ and $\hat{G}_{\text{bla},31}$.

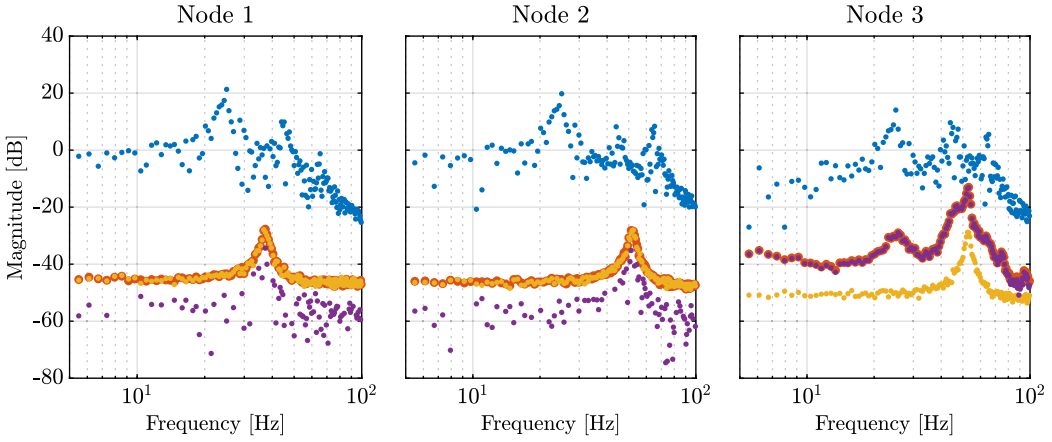

Fig. 9. Nonlinearity detection in the three-mass–spring-damper system using the node-to-node dynamics. The spectra of the node signals $y_i(\omega_k)$ (•), the total distortion levels $\sigma^2_{t,i}(\omega_k)$ (•), the distortions due to noise $\sigma^2_{v,i}(\omega_k)$ (•), and the nonlinear distortions $\sigma^2_{s,i}(\omega_k)$ (•), are depicted. Dominant nonlinear dynamics are observed at the third node since the nonlinear distortion is larger than the noise distortion.

6. Experimental validation

This section demonstrates the nonlinearity location methodology from Section 4 applied to the flexible beam system from Fig. 10. The beam is 500 × 20 × 2 mm, is suspended with wire flexures, and is actuated with three current-driven voice-coil actuators. The deflection is measured with five contactless fiberoptic sensors. The outer two and the middle sensor are used for the following experiment. A schematic drawing is depicted in Fig. 11, which illustrates the free degrees of freedom. Next to the internal deformation, the beam can translate and is free to rotate, see [45] for further details.

By means of an artificial control loop, a nonlinear cubic spring force is added between the fixed world and the third actuator–sensor pair. This is done by manipulating the third input as

$$u_3 = u_{3,\mathrm{o}} - k_{\mathrm{nl}} \left(y_3 - y_{3,\mathrm{r}} \right)^3 , \tag{42}$$

where u_3 is the applied input, $u_{3,\mathrm{o}}$ is the non-manipulated input, and $y_{3,\mathrm{r}}$ is the relaxed position of the cubic spring. Similar to the numerical demonstration from Section 5, multisine signals are simultaneously applied to the three masses which excite the system in the 0.25–500 Hz band with a root-mean-square amplitude of 0.02 A. The system is measured at 4096 Hz and $\tilde{M} = 6$ experiments are repeated over $\tilde{P} = 6$ periods of 4 s of which the last $P = 3$ steady state periods are used. These measurements are repeated for three different cubic spring constants where $k_{\mathrm{nl}} \in \{0, 1, 10\}$.

To be able to perform the nonlinearity location, the networked BLA setting is considered. As the system under test in this case is a distributed system, and not a lumped system such as the numerical example in Section 5, a dense network with dynamic interconnections between every node is considered. This particular network structure is depicted in Fig. 5. Each of the output measurements corresponds to one of the network nodes and each node is excited by u_i through the submodel G_{u_i}.

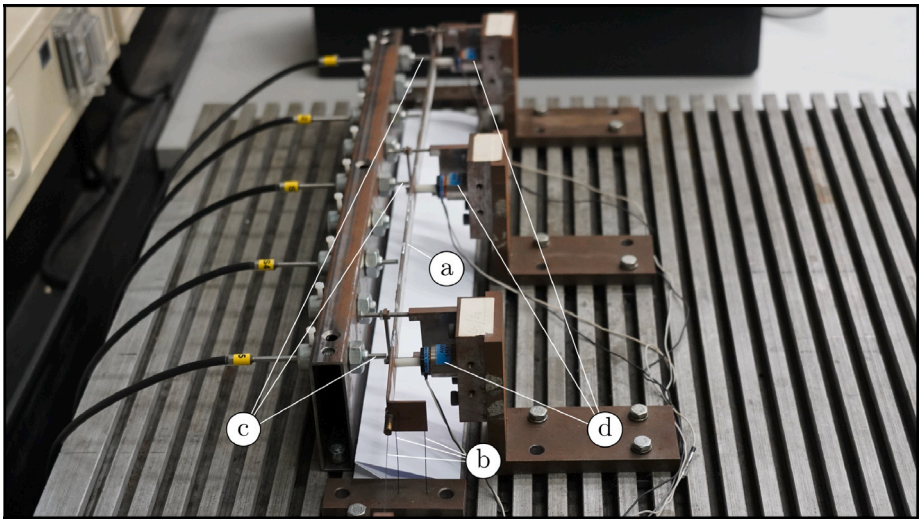

Fig. 10. Prototype experimental flexible beam setup. The moving part is indicated by (a) and is suspended by wire flexures (b). The deflection is measured with five contactless fiberoptic sensors of which three are used (c) and the setup is actuated with three current-driven voice coils (d). A cubic stiffness is artificially added between fixed world and the third actuator–sensor pair.

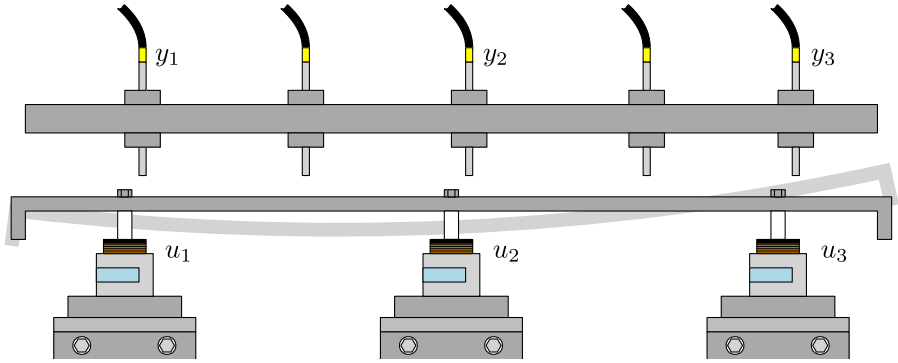

Fig. 11. Visualization of the flexible beam setup from Fig. 10. The actuator and sensor locations are indicated by u_i and y_i respectively. During excitation, the beam translates, rotates, and exhibits flexible behavior.

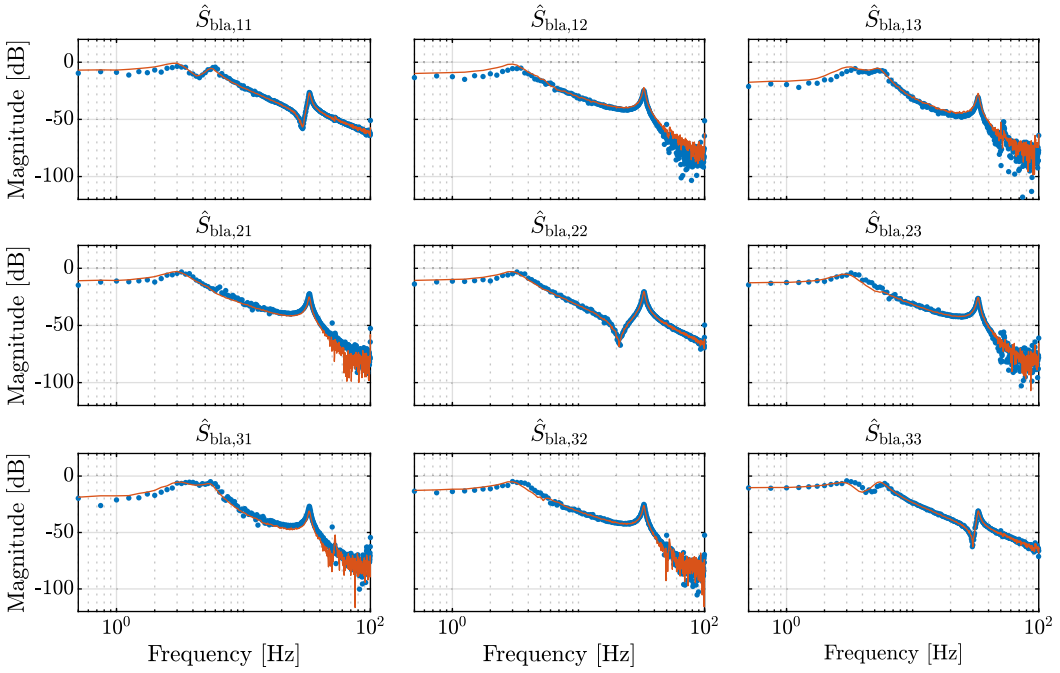

Fig. 12. The BLA from the inputs to nodes $\hat{S}_{\text{bla}}$ (•) obtained for the $k_{\text{nl}} = 1$ setting and a FRF measured of the system without nonlinearity, i.e., $\hat{S}$ with $k_{\text{nl}} = 0$ (—).

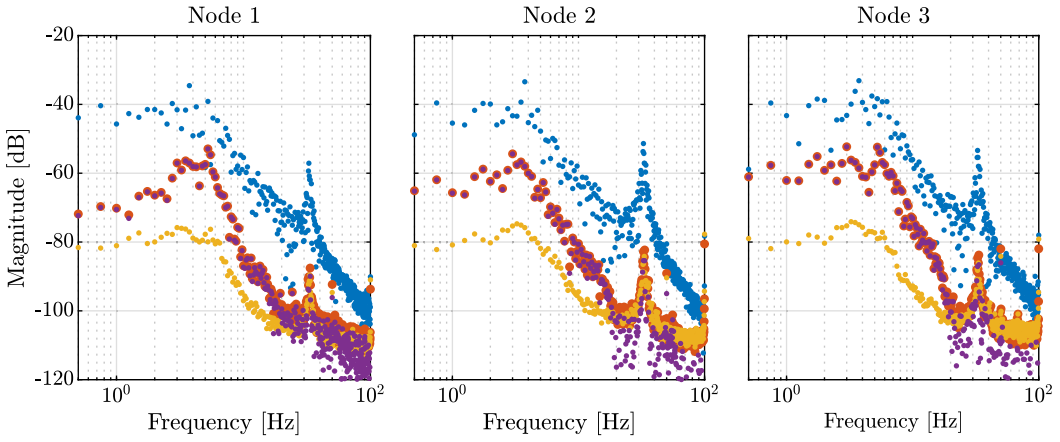

Fig. 13. Nonlinearity detection in the flexible beam system with $k_{\text{nl}} = 1$ using the classical MIMO BLA approach with input-to-node dynamics. The spectra of the node signals $y_i(\omega_k)$ (•), the total distortion levels $\sigma^2_{t,i}(\omega_k)$ (•), the distortions due to noise $\sigma^2_{v,i}(\omega_k)$ (•), and the nonlinear distortions $\sigma^2_{s,i}(\omega_k)$ (•), are depicted. Since the nonlinear distortion is above the noise floor, dominant nonlinearity is detected in the system. Pinpointing the precise location is not possible using the classical approach.

In the first step, the BLA estimate $\hat{S}_{\text{bla}}$ is calculated from inputs to the nodes using the robust BLA method, that is, using (28). This BLA is depicted in Fig. 12 for the $k_{\text{nl}} = 1$ case. The first resonance relates to the wire flexures that suspend the beam and the second resonance around 32.5 Hz is the first internal mode of the beam.

A naive nonlinearity analysis from input to node, as is done by the classical MIMO BLA framework, results in the detection of nonlinearity in all three measurement locations, as shown in Fig. 13. Although such an analysis allows for the detection and quantification of the nonlinearity present in the system, it clearly does not allow to pinpoint the location of the nonlinearity since the nonlinear distortion is larger than the noise distortion at every node.

Finally, the three-step approach for detection, location, and quantification of Section 4.4 is applied. Using these networked BLAs, a detailed distortion analysis at the node level is possible in a networked setting. The results depicted in Figs. 14–16 for $k_{\text{nl}} = 0$, $k_{\text{nl}} = 1$, and $k_{\text{nl}} = 10$ respectively.

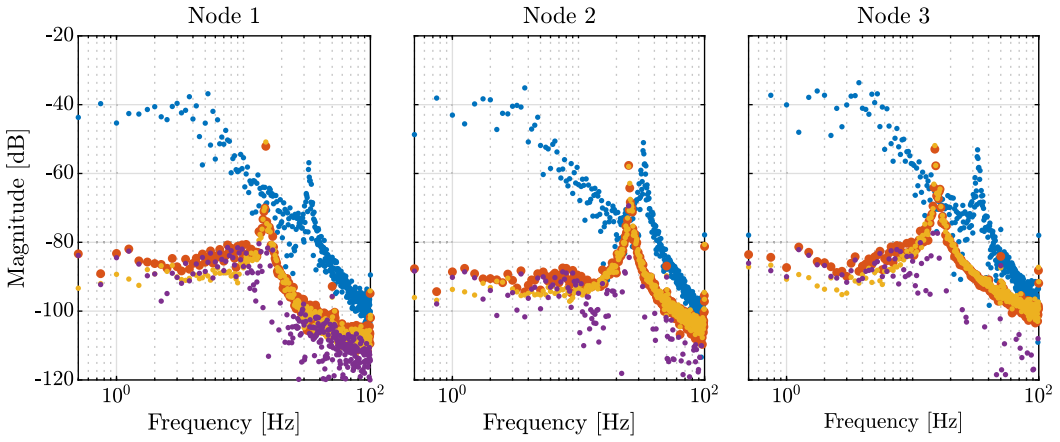

Fig. 14. Networked BLA nonlinearity analysis on the measurement nodes obtained for the $k_{\mathrm{nl}} = 0$ setting. The spectra of the node signals $y_i(\omega_k)$ (•), the total distortion levels $\sigma^2_{t,i}(\omega_k)$ (•), the distortions due to noise $\sigma^2_{v,i}(\omega_k)$ (•), and the nonlinear distortions $\sigma^2_{s,i}(\omega_k)$ (•), are depicted. No dominant nonlinear dynamics are observed since the noise distortion has a higher or equal contribution with respect to the nonlinear distortion.

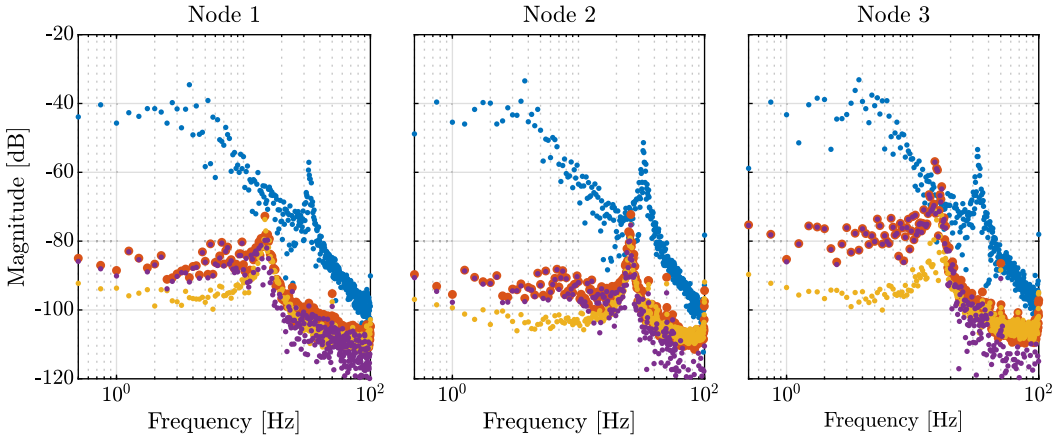

Fig. 15. Networked BLA nonlinearity analysis on the measurement nodes obtained for the $k_{\mathrm{nl}} = 1$ setting. The spectra of the node signals $y_i(\omega_k)$ (•), the total distortion levels $\sigma^2_{t,i}(\omega_k)$ (•), the distortions due to noise $\sigma^2_{v,i}(\omega_k)$ (•), and the nonlinear distortions $\sigma^2_{s,i}(\omega_k)$ (•), are depicted. Dominant nonlinear dynamics are observed at the third node because the nonlinear distortion is significantly above the noise distortion.

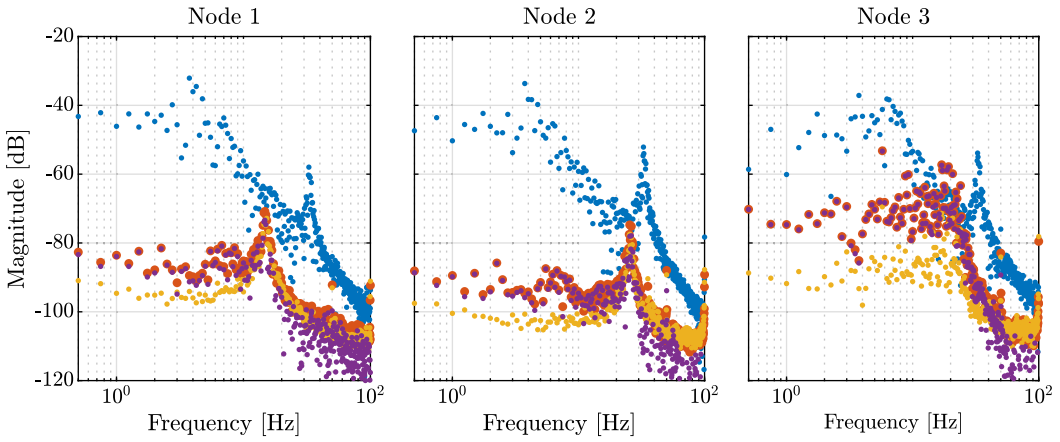

Fig. 16. Networked BLA nonlinearity analysis on the measurement nodes obtained for the $k_{\mathrm{nl}} = 10$ setting. The spectra of the node signals $y_i(\omega_k)$ (•), the total distortion levels $\sigma^2_{t,i}(\omega_k)$ (•), the distortions due to noise $\sigma^2_{v,i}(\omega_k)$ (•), and the nonlinear distortions $\sigma^2_{s,i}(\omega_k)$ (•), are depicted. An increased nonlinear distortion is observed at the third node since the magnitude is higher compared to Fig. 15.

Without nonlinear spring, i.e., $k_{nl} = 0$, no dominant source of nonlinearity is detected because the noise distortion is almost equal to the total distortion in Fig. 14. In contrast to the numerical example provided in Section 5, some weak low-frequency nonlinearity is detected. This distortion is most likely attributed to other non-idealities that are present in the setup. When the nonlinear spring stiffness is increased to $k_{nl} = 1$, a ~10 dB clearance is observed between the estimated noise level and the nonlinear distortion at the third node, see Fig. 15. Furthermore, the nonlinearity is mainly active at the resonance frequency associated to the third node. This corresponds to the presence of a nonlinear spring at that location in the physical setup. In case $k_{nl} = 10$, see Fig. 16, the magnitude is even larger indicating a nonlinearity of larger magnitude. In conclusion, the proposed algorithm does not only locate the nonlinearity, but also quantifies the nonlinearity over the considered frequency range.

7. Conclusion

This paper presents a non-parametric frequency domain approach to locate nonlinearities and quantify its magnitude. The nonlinear system is conceptualized as a dynamic network and a residual analysis is conducted based on residuals between the measurement data and the linearized node-to-node dynamics. The graphical output consists of frequency-domain graphs per measurement location, allowing to easily detect and pinpoint the origin of the nonlinear behavior, which is essential during the system design phase and after commissioning machines for the purpose of fault detection and isolation. The efficacy of the proposed approach is demonstrated through numerical simulations and experimental validation. In conclusion, this approach offers a systematic and quantitative means to evaluate the impact of nonlinearity across a broad spectrum of nonlinear systems.

CRediT authorship contribution statement

Koen Classens: Writing – review & editing, Writing – original draft, Visualization, Validation, Software, Methodology, Investigation, Conceptualization. **Maarten Schoukens:** Writing – review & editing, Software, Methodology, Funding acquisition, Conceptualization. **Tom Oomen:** Writing – review & editing, Supervision, Funding acquisition. **Jean-Philippe Noël:** Writing – review & editing, Software, Methodology, Funding acquisition, Conceptualization.

Declaration of competing interest

The authors declare that they have no known competing financial interests or personal relationships that could have appeared to influence the work reported in this paper.

Acknowledgments

This work is supported by ASML Research, Veldhoven, the Netherlands. In addition, this work is funded by the European Union (Horizon Europe, ERC, COMPLETE, 101075836). Views and opinions expressed are however those of the author(s) only and do not necessarily reflect those of the European Union or the European Research Council Executive Agency. Neither the European Union nor the granting authority can be held responsible for them.

Data availability

Data will be made available on request.

References

[1] G. Kerschen, K. Worden, A.F. Vakakis, J. Golinval, Past, present and future of nonlinear system identification in structural dynamics, Mech. Syst. Signal Process. 20 (3) (2006) 505–592.
[2] A.F. Vakakis, O.V. Gendelman, L.A. Bergman, D.M. McFarland, G. Kerschen, Y.S. Lee, Nonlinear Targeted Energy Transfer in Mechanical and Structural Systems, Springer Science & Business Media, 2008.
[3] P. Green, K. Worden, K. Atallah, N. Sims, The benefits of Duffing-type nonlinearities and electrical optimisation of a mono-stable energy harvester under white Gaussian excitations, J. Sound Vib. 331 (20) (2012) 4504–4517.
[4] D.D. Quinn, A.L. Triplett, A.F. Vakakis, L.A. Bergman, Energy harvesting from impulsive loads using intentional essential nonlinearities, J. Vib. Acoust. 133 (1) (2011) 011004.
[5] H. Nijmeijer, A. van der Schaft, Nonlinear Dynamical Control Systems, Springer New York, 1990.
[6] A. Isidori, Nonlinear Control Systems, Springer London, 2013.
[7] K. Classens, J. van de Wijdeven, W.P.M.H. Heemels, T. Oomen, Opportunities of digital twins for high-tech systems: From fault diagnosis and predictive maintenance to control reconfiguration, Mikroniek 63 (5) (2023) 5–12.
[8] K. Classens, W.P.M.H. Heemels, T. Oomen, Digital twins in mechatronics: From model-based control to predictive maintenance, in: 2021 IEEE 1st International Conference on Digital Twins and Parallel Intelligence, DTPI, 2021, pp. 336–339.
[9] D.J. Ewins, B. Weekes, A. delli Carri, Modal testing for model validation of structures with discrete nonlinearities, Philos. Trans. R. Soc. Lond. Ser. A Math. Phys. Eng. Sci. 373 (2051) (2015) 20140410.
[10] A. delli Carri, B. Weekes, D. Di Maio, D.J. Ewins, Extending modal testing technology for model validation of engineering structures with sparse nonlinearities: A first case study, Mech. Syst. Signal Process. 84 (2017) 97–115.
[11] J. Swevers, F. Al-Bender, C. Ganseman, T. Prajogo, An integrated friction model structure with improved presliding behavior for accurate friction compensation, IEEE Trans. Autom. Control 45 (4) (2000) 675–686.

[12] M. Ruderman, T. Bertram, M. Iwasaki, Modeling, observation, and control of hysteresis torsion in elastic robot joints, Mechatronics 24 (5) (2014) 407–415.
[13] J.P. Noël, L. Renson, G. Kerschen, Complex dynamics of a nonlinear aerospace structure: Experimental identification and modal interactions, J. Sound Vib. 333 (12) (2014) 2588–2607.
[14] P. Csurcsia, J. Decuyper, B. Renczes, M. Runacres, T. De Troyer, Reducing black-box nonlinear state-space models: A real-life case study, Mech. Syst. Signal Process. 211 (2024) 111230.
[15] Y. Yuan, G.-B. Stan, S. Warnick, J. Goncalves, Robust dynamical network structure reconstruction, Automatica 47 (6) (2011) 1230–1235.
[16] P.M.J. Van den Hof, A. Dankers, P.S.C. Heuberger, X. Bombois, Identification of dynamic models in complex networks with prediction error methods - basic methods for consistent module estimates, Automatica 49 (10) (2013) 2994–3006.
[17] P.M.J. Van den Hof, A. Dankers, H.H. Weerts, Identification in dynamic networks, Comput. Chem. Eng. 109 (2018) 23–29.
[18] A. Dankers, P.M.J. Van den Hof, X. Bombois, P.S.C. Heuberger, Identification of dynamic models in complex networks with prediction error methods: Predictor input selection, IEEE Trans. Autom. Control 61 (4) (2016) 937–952.
[19] J. Goncalves, S. Warnick, Necessary and sufficient conditions for dynamical structure reconstruction of LTI networks, IEEE Trans. Autom. Control 53 (7) (2008) 1670–1674.
[20] A. Chiuso, G. Pillonetto, A Bayesian approach to sparse dynamic network identification, Automatica 48 (8) (2012) 1553–1565.
[21] D. Materassi, G. Innocenti, Topological identification in networks of dynamical systems, IEEE Trans. Autom. Control 55 (8) (2010) 1860–1871.
[22] J. Noël, G. Kerschen, Nonlinear system identification in structural dynamics: 10 more years of progress, Mech. Syst. Signal Process. 83 (2017) 2–35.
[23] S. Marchesiello, L. Garibaldi, A time domain approach for identifying nonlinear vibrating structures by subspace methods, Mech. Syst. Signal Process. 22 (2008) 81–101.
[24] J. Noël, G. Kerschen, Frequency-domain subspace identification for nonlinear mechanical systems, Mech. Syst. Signal Process. 40 (2013) 701–717.
[25] M. Schoukens, P.M.J. Van den Hof, Detecting nonlinear modules in a dynamic network: A step-by-step procedure, IFAC-PapersOnLine 51 (15) (2018) 593–597.
[26] J. Schoukens, R. Pintelon, Y. Rolain, M. Schoukens, K. Tiels, L. Vanbeylen, A. Van Mulders, G. Vandersteen, Structure discrimination in block-oriented models using linear approximations: A theoretic framework, Automatica 53 (2015) 225–234.
[27] M. Schoukens, K. Tiels, Identification of block-oriented nonlinear systems starting from linear approximations: A survey, Automatica 85 (2017) 272–292.
[28] A. Josefsson, M. Magnevall, K. Ahlin, G. Broman, Spatial location identification of structural nonlinearities from random data, Mech. Syst. Signal Process. 27 (2012) 410–418.
[29] G. Kosova, E. Di Lorenzo, B. Peeters, G. Kerschen, Locating structural nonlinearities using linear frequency response functions and nonlinear orthogonal projections, Mech. Syst. Signal Process. 202 (2023) 110585.
[30] J. Schoukens, T. Dobrowiecki, R. Pintelon, Parametric and non-parametric identification of linear systems in the presence of nonlinear distortions. A frequency domain approach, IEEE Trans. Autom. Control 43 (2) (1998) 176–190.
[31] R. Pintelon, J. Schoukens, System Identification: A Frequency Domain Approach, Wiley-IEEE Press, 2012.
[32] E. Wernholt, S. Gunnarsson, Estimation of nonlinear effects in frequency domain identification of industrial robots, IEEE Trans. Instrum. Meas. 57 (4) (2008) 856–863.
[33] M. Vaes, J. Schoukens, B. Peeters, J. Debille, T. Dossogne, J. Noël, C. Grappasonni, G. Kerschen, Nonlinear ground vibration identification of an F-16 aicraft - Part 1: Fast nonparametric analysis of distortions in FRF measurements, in: Proceedings of the International Forum on Aeroelasticity and Structural Dynamics, IFASD, 2015.
[34] T. Dobrowiecki, J. Schoukens, Measuring a linear approximation to weakly nonlinear MIMO systems, Automatica 43 (10) (2007) 1737–1751.
[35] T. Dobrowiecki, J. Schoukens, Linear approximation of weakly nonlinear MIMO systems, IEEE Trans. Instrum. Meas. 56 (3) (2007) 887–894.
[36] R. Pintelon, J. Schoukens, The best linear approximation of nonlinear systems operating in feedback, in: 2012 IEEE International Instrumentation and Measurement Technology Conference Proceedings, 2012, pp. 2092–2097.
[37] R. Pintelon, J. Schoukens, FRF Measurement of Nonlinear Systems Operating in Closed Loop, IEEE Trans. Instrum. Meas. 62 (5) (2013) 1334–1345.
[38] M. Schoukens, R. Pintelon, T.P. Dobrowiecki, J. Schoukens, Extending the best linear approximation framework to the process noise case, IEEE Trans. Autom. Control 65 (4) (2020) 1514–1524.
[39] A. Dankers, System Identification in Dynamic Networks (Ph.D. thesis), Eindhoven University of Technology, 2014.
[40] E. Kivits, Modelling and Identification of Physical Linear Networks (Ph.D. thesis), Eindhoven University of Technology, 2024.
[41] S. Boyd, L. Chua, Fading memory and the problem of approximating nonlinear operators with Volterra series, IEEE Trans. Circuits Syst. 32 (11) (1985) 1150–1161.
[42] J. Schoukens, M. Vaes, R. Pintelon, Linear system identification in a nonlinear setting: Nonparametric analysis of the nonlinear distortions and their impact on the best linear approximation, IEEE Control Syst. 36 (3) (2016) 38–69.
[43] P.Z. Csurcsia, B. Peeters, J. Schoukens, User-friendly nonlinear nonparametric estimation framework for vibro-acoustic industrial measurements with multiple inputs, Mech. Syst. Signal Process. 145 (2020) 106926.
[44] M. Geradin, D. Rixen, Mechanical Vibrations: Theory and Application to Structural Dynamics, Wiley, 2015.
[45] K. Classens, W.P.M.H. Heemels, T. Oomen, A closed-loop perspective on fault detection for precision motion control: With application to an overactuated system, in: 2021 IEEE International Conference on Mechatronics, ICM, 2021.